D'Auria Luca (Orcid ID: 0000-0002-7664-2216)

Pérez Nemesio M. (Orcid ID: 0000-0003-1410-7717)

Padrón Eleazar (Orcid ID: 0000-0003-3907-5766)

The 2016 Tenerife (Canary Islands) long-period seismic swarm

Luca D'Auria (1,2), José Barrancos (1,2), Germán D. Padilla (1,2), Nemesio M. Pérez (1,2,3), Pedro A. Hernández (1,2,3), Gladys Melián (1,2,3), Eleazar Padrón (1,2,3), María Asensio-Ramos (1), Rubén García-Hernández (1)

(1) Instituto Volcanológico de Canarias (INVOLCAN), Calle Álvaro Martín Díaz 2, 38320 San Cristóbal de la Laguna, Tenerife, Canary Islands, Spain

(2) Instituto Tecnológico y de Energías Renovables (ITER), 38600 Granadilla de Abona, Tenerife, Canary Islands, Spain

(3) Agencia Insular de la Energía de Tenerife (AIET), 38600 Granadilla de Abona, Tenerife, Canary Islands, Spain

Key points

- On 2 October 2016 a significant seismic swarm of more than 766 long-period events, that lasted more than 5 hours, was recorded on Tenerife.
- The seismological features of the swarm point to an unsteady choked flow, due to a massive fluid release, as a possible source mechanism.
- The swarm was followed by an increase in the diffuse CO_2 emission and by an increase in the volcano-tectonic seismicity.

This article has been accepted for publication and undergone full peer review but has not been through the copyediting, typesetting, pagination and proofreading process which may lead to differences between this version and the Version of Record. Please cite this article as doi: 10.1029/2019JB017871

Abstract

On 2 October 2016, a significant seismic swarm of long-period events was recorded on Tenerife (Canary Islands, Spain). The swarm lasted more than 5 hours and consisted of at least 766 detected events. We found a positive correlation between the amplitude of each event and the preceding inter-event time together with a stability of the spectral properties and waveform similarity during most of the swarm duration. Towards the end of the swarm, individual events merged into a continuous tremor.

These observations can be explained by postulating an unsteady transonic choked flow within a crack-like conduit as a source mechanism for this swarm. The flow resulted from a sudden discharge of magmatic fluids from a pressurized reservoir into the hydrothermal system of Tenerife. The injected fluids reached the surface starting about one month after the swarm, as evidenced by the macroscopic increase in the diffuse CO_2 emissions from the crater of Teide volcano.

The lack of ground deformation and the absence of relevant seismicity at depths greater than 10 km, excludes the ascent of a basaltic magma batch as a causative source mechanism. Instead we hypothesize the sudden release of fluids accumulated at the top of a magma chamber as a possible mechanism. Another possibility is the injection of a small batch of mafic magma into a cooling magma chamber, triggering a convective mixing. Both cases imply the presence of a magma chamber at depths greater than 8.6 km. These results have important implications for the development of the volcano monitoring system of Tenerife.

Key words

- Long-period events
- Hydrothermal system
- Tenerife
- Teide volcano
- Volcanic unrest

Introduction

The volcanic archipelago of the Canary Islands, evolved during the last 70-80 Ma because of the interaction of a mantle plume with tectonic structures linked to the NW margin of the African plate (Anguita & Hernán, 2000). The island of Tenerife developed, starting about 6.5 Ma ago, with the building of three shield volcanoes (Ancochea et al., 1990). A subsequent phase, which began 3.5 Ma ago, led to the formation of the Las Cañadas volcanic complex at the center of the island, which underwent at least three distinct building stages (Ancochea et al., 1990; Ancochea et al., 1999). The evolution of the Las Cañadas complex included a sequence of collapses, the last one occurring 0.2 Ma, which led to the formation of the current Las Cañadas caldera (Ancochea at al., 1999; Carracedo et al., 2007). The last phase, starting 0.15 Ma, formed the Teide-Pico Viejo stratovolcano (TPV), currently the most prominent volcanic edifice of the island (Fig. 1) (Ancochea et al., 1999). Other relevant phenomena, relative to the volcano-tectonic evolution of the island, were massive gravitational flank collapses (Hurlimann et al., 1999).

The Pleistocene volcanic activity was concentrated on the three radial rifts: North-East (NE), North-West (NW) and North-South (N-S) as well as the TPV (Carracedo et al., 2007) (Fig. 1). During the Holocene, eruptions occurred along the NE and NW rifts as well as on the TPV. Historical eruptions were recorded on 1704-1705 (Arafo-Fasnia-Siete Fuentes; NE rift), 1706 (Garachico; NW rift), 1798 (Narices del Teide; TPV) and 1909 (Chinyero; NW rift) (Romero, 1991).

The current volcanic activity of the island of Tenerife consists in a volcanic degassing, from fumaroles on the summit cone of Teide volcano but mostly as well as diffuse soil degassing from the whole volcanic edifice. Furthermore, background microseismicity is continuously observed beneath the island (Melián et al., 2012; Pérez et al., 2013). Between 2004 and 2005, an increase in the seismicity was accompanied by geochemical anomalies and a moderate ground uplift (Gottsmann et al., 2006; Peréz et al., 2007; Almendros et al., 2007; Fernández et al., 2009; Martí et al., 2009; Domínguez et al., 2011; Melián et al., 2012). This minor seismo-volcanic unrest has been interpreted as a result of a small magmatic intrusion with subsequent release of magmatic gases which perturbed the hydrothermal system of the island.

On 2 October 2016, starting at around 13:16 UTC, various seismic stations deployed on the island recorded a remarkable seismic swarm of long-period events (hereinafter referred to as 2OSS) lasting at least until 18:34 UTC. The swarm consisted of at least 766 discrete events, although during the initial and final phase, discrete events overlapped forming a continuous volcanic tremor.

In the following we present a seismological analysis of this swarm, comparing it with other seismological and geochemical data to infer about the possible source mechanism(s) and its implication about the dynamics of the volcano.

Data

In June 2016, the *Instituto Volcanológico de Canarias* (INVOLCAN) started the deployment of the Red Sísmica Canaria (FDSN code C7; http://doi.org/doi:10.7914/SN/C7). The first phase of installation was completed on November 20, 2016. During the 2OSS the only fully operative seismic station was TNOR (Fig. 1). All the stations of C7 are equipped with Nanometrics® Trillium Compact 120 s broadband seismic sensors with a 100 Hz sampling frequency. We also used the waveforms of the station MACI (Fig. 1), available on IRIS Data Services.

Using the software Drum_Pkev (Giudicepietro et al., 2010) we manually picked the onset of 766 long-period events within the swarm. Picking was realized on high-pass filtered (> 1Hz) waveforms of the N-S component of TNOR, which was the one having the higher signal/noise ratio.

To locate the hypocenter of the source we also used the seismic phases of CCAN and CBOL stations (Fig. 1), operated by the *Instituto Geográfico Nacional* (IGN).

The 2 October 2016 seismic swarm

The first detectable event of the 2OSS occurs at 13:16:39 UTC (Fig. 2B). After this first small-amplitude event, the spectrogram shows continuous spectral lines, possibly indicating a weak volcanic tremor (Fig. 2B). After around 13:30 UTC discrete events start to be more clearly distinguishable, until they become clearly separated after about 14:00 UTC. The sequence of these repeating events lasts without interruptions until 17:55 UTC (Fig. 2C and 2D). At this moment the events start to be closely overlapped, leading to a clear volcanic tremor signal, with some discrete events still distinguishable from the background (Fig. 2D). The last discrete event is detected at 18:34 UTC. The volcanic tremor amplitude progressively wanes, disappearing after 19:00 UTC (Fig. 2D). In the supplementary figure S1 we represent the whole swarm in a helicorder plot.

The overall spectral features of the 2OSS show dominant amplitudes in the range 2-8 Hz, with marked spectral peaks, persisting along the whole duration of the swarm (Fig. 2A). Furthermore, the spectrogram evidenced a nearly stationary spectrum also during the transition from discrete events to continuous tremor (Fig. 2D).

In figure 3B we report the evolution of the inter-event times during the swarm. It starts with values below 20 s, progressively increasing to average values of about 30 s after 14:00 UTC. The inter-event times continues increasing reaching an average value of about 50 s, before suddenly dropping at 17:55 UTC, at the onset of the volcanic tremor (Fig. 3B).

The statistical distribution of the inter-event times is definitely non-Poissonian. This is in striking contrast with the worldwide statistics of volcano-tectonic earthquakes inter-event times which, conversely, shows generally a Poissonian distribution (Bottiglieri et al., 2009). Following Bell et al. (2017) we define the periodicity as the ratio between the average and the standard deviation of inter-event times over moving average windows. For a genuinely Poissonian inter-event times distribution, periodicity should be close to 1. In figure 3A we show the periodicity computed both on 10 min and 30 min moving windows. They clearly show for most of the time, values higher than one, indicating a repetitive source mechanism for the 2OSS.

The spectral features of these events, their repetitive waveforms and their high periodicity are features commonly observed in other swarms of long-period events, which are sometimes also called “hybrid” events on the basis of the presence of an high frequency component or “drumbeat” events because of their regularity (Martini et al., 2007; Matoza et al., 2009, 2010; Bell et al., 2017). In the following we analyze some of the relevant features of individual events: amplitude, spectral content, waveform similarity to infer the nature of their seismic source.

The amplitudes of discrete events (Fig. 3C), represent the maximum of the Euclidean norm of the three components of the station TNOR. They show a temporal evolution which resembles closely that of the inter-event times. In figure 3D we show a graph with the correlation between the logarithm of the amplitudes and of the logarithm of the inter-event times. We performed a robust fit using the RANSAC algorithm (RANdom SAmple Consensus) (Fischler & Bolles, 1981). The result clearly shows a positive correlation between these two quantities. The outliers, discarded by the RANSAC algorithm, have been represented in red and green in figures 3B, 3C and 3D. It is worth to mention that most of them are grouped around 18:00 UTC, during the transition between discrete events and continuous tremor. This group is characterized by short inter-event times and a relatively larger amplitude. Therefore, we conclude that the positive correlation between amplitude and inter-event interval, points to some nondestructive source mechanism involving a recharge process. A similar feature was observed in long-period events recorded during 2004-2005 at Mt. St. Helens (Matoza and Chouet, 2010).

Complex spectral analysis

The complex spectral analysis is one of the most powerful tools in volcano seismology: it allows inferring about the physical property of the source of long-period events, putting constraint on its geometry and on the nature of the fluid filling the resonating fractures (Kumagai & Chouet, 1999; Chouet, 2003; Chouet & Matoza, 2013). We applied the Sompi method to extract the complex spectral components from the seismogram of individual events (N-S component of TNOR), using autoregressive coefficients with orders ranging from 4 to 60 and a folding factor of 5 (Hori et al., 1989; Nakano et al., 1998). For each event we selected the window starting from the maximum amplitude peak and having a duration of 20 s. In figure 4 we represent the density of complex spectral components (Fig. 4C) as well as histograms with the distribution of frequencies (Fig. 4A) and quality factors (Fig. 4B). The frequencies show two peaks for values of 3.9 and 5.2 Hz. The analysis of the power spectrum shows that, at least the 3.9 Hz peak, is not caused by site effects but is related to the seismic source. In fact, this peak is common to both stations and does not appear in the background noise (see figures S2 and S3 in supplementary material).

The analysis of the temporal variation of the complex frequencies shows that the frequency is nearly constant, while the quality factors show remarkable variations (Fig. 5). In figure 5B we show the temporal variations of the quality factor of all the spectral components, while in figure 5C we show only those related to the 3.9 Hz frequency peak. Both show a slight decrease in the first phase of the swarm, becoming nearly constant at about 14:00 UTC, with values ranging generally from 20 to 70. With the onset of the continuous tremor at 17:55 UTC (Fig. 2D), both the frequency and the quality factor show a sudden change (Fig. 5). Frequencies appear to be more uniformly distributed, while the quality factor increases to values ranging between 40 and 300.

Waveform clustering and hypocenter location

Using the waveforms of individual events, we computed the cross-correlation matrix among waveforms (see supplementary figure S4). The waveforms used for the analysis, taken from the N-S component of TNOR station, have a length of 5 s starting from the event onset. The cross-correlation matrix shows, in general, a high level of similarity among the waveforms, with cross-correlation values generally higher than 0.8 among event pairs. We performed a clustering analysis using the Density-Based Spatial Clustering of Applications with Noise (DBSCAN) algorithm (Ester et al., 1996). This algorithm joins together points having a distance less than a threshold ε and considering also a minimum number of neighbors when creating clusters. The metric used for this analysis is based on the maximum cross-correlation value:

$$d_{ij} = \frac{1-c_{ij}}{c_{ij}},$$

where d_{ij} is the distance between events i and j, and c_{ij} is the corresponding maximum of the cross-correlation. In our application of DBSCAN we used a minimum distance threshold ε corresponding to a cross-correlation value of 0.9 and a minimum number of neighbors of 5. The clustering analysis revealed the presence of a large single cluster of 417 events and 349 orphan events. In figure 6 we indicate with different colors the events belonging or not to the cluster. It can be seen that most of the orphan events are concentrated in the initial and final phases of the seismic swarm.

In figure 6 we represent the aligned waveforms for the three components of TNOR, for the 417 events belonging to the cluster. They show a very high similarity, with minor variations due mostly to the presence of the noise. We stacked the aligned individual waveforms, obtaining signals where the onset of P and S phases is clearly visible (Fig. 6B-D-F). The same procedure has been applied to the waveforms of the MACI station. This allowed determining the S-P travel time difference on both stations, and the difference between S travel times of the two stations.

To locate the hypocenter of the centroid for the events belonging to the swarm, we assumed the P-wave arrival at MACI as a time reference. Since for the stations CCAN and CBOL only arrival time pickings were available, we computed the average difference between the P and S phases of these two stations and the P arrival time at MACI for all the events of the swarm where both phases were available. This allowed to compute also the P and S relative arrival times of CCAN and CBOL with respect to the P phase of MAC.

To compute the hypocenter, we used the NonLinLoc software, which is based on a non-linear probabilistic approach (Lomax et al., 2000). In particular, we used the Equal-Differential-Time method to determine the maximum-likelihood hypocenter as well as the whole "*a posteriori*" probability density function (Font et al., 2004). We remark that this single hypocenter is representative of all individual events of the swarm since we assume, they share the same source position, within the experimental uncertainty. This hypocenter is located on the SW rim of Las Cañadas caldera, at a depth of about 8.6 km b.s.l. (Fig. 7). In figure 7 we represent, together with the maximum-likelihood hypocenter position, also the full "*a posteriori*" p.d.f. This function is represented as small red points whose density is proportional to the p.d.f. value. We observe that the pd.f. shape is elongated along the N-S direction. This is due to the position of the seismic stations used for the location which are more or less aligned along an E-W direction. The uncertainty over the epicenter position is 3.6 km, while for the depth is 2.1 km. The velocity model used for the location is the 1D model proposed by García-Yeguas et al. (2012).

Discussion

The most striking feature of the 2OSS is the presence of repeating events with highly similar waveforms. This is a feature commonly observed on other active volcanoes such as Redoubt (Chouet, 2003), Stromboli (Martini et al., 2007), Mount St. Helens (Matoza et al., 2009; Matoza and Chouet, 2010), Campi Flegrei (Cusano et al., 2008) and Tungurahua (Bell et al., 2017). They have generally been related to volcanic degassing processes.

The repeating event waveforms are linked to a non-destructive mechanism which allows the transients to repeat in a nearly unchanged source. Furthermore, the relationship between the amplitude of each event, and the preceding inter-event time (Fig. 3D) highlight the presence of some kind of recharge mechanisms, in which the energy progressively accumulates between successive events. Another important feature of this swarm is the sudden transition towards a nearly continuous tremor (Fig. 2D) associated to a change in the characteristics of the waveforms, as evidenced by the complex spectral analysis and the cross-correlation matrix (Fig. 5).

A plausible source mechanism, which might explain all the observed phenomenology, is that of an unsteady transonic choked flow within a crack-like conduit. This mechanism has been exhaustively studied by Morrissey and Chouet (1997) and has been often invoked as a source mechanism for repeating long-period events swarm (Chouet, 2003; Chouet and Matoza, 2013). Transonic fluid flow in a crack-like conduit presenting width variations leads to the formation of oblique shock fronts within the conduit. These fronts hinder the fluid flow through the conduit, causing the development of a pressure gradient. Once the pressure gradient exceeds a threshold, the shock is disrupted, causing the pressure gradient to drop suddenly. This abrupt pressure change is the source of the damped oscillations of the fluid-filled crack or, in other words, of the individual long-period events.

In our case, this mechanism, would be able to explain the positive correlation between amplitudes and inter-event times. Actually, the intensity of the pressure drop clearly depends on the inter-event time, being the build-up of the pressure behind the shocks continuously increasing with time.

This mechanism is also able to explain the initial and final transitions from and to a continuous tremor. In fact, the chocked flow mechanism is strongly dependent on the conduit geometry and on pressure gradients. The initial gradual onset of the swarm, is likely to be related to the progressive opening of a crack, in which high-pressure fluids were being injected. On the other hand, the transition towards a continuous tremor at 17:55 UTC, may be related to the decrease of the pressure gradient because of a re-equilibration process. In other words, the fluid transfer from the pressurized reservoir to the hydrothermal system of the volcano, caused a progressive reduction of

the initial, stronger, pressure gradients. As shown by Morrisey and Chouet (1997), below a critical threshold of the pressure gradient, the nearly regular transients of the choked flow turn into chaotic, nearly continuous, oscillations.

In many volcanoes, despite missing evident surface hydrothermal manifestations (fumarole, hot pools, etc.), the diffuse gas emission is the dominant degassing mechanism (Hernández et al., 1998). Diffuse degassing of volcanic origin has been measured in different areas of interest in Tenerife and has been related with the dynamics of the volcanic system (Pérez et al., 2013; Hernández et al., 2017). Since 1999, time series of CO_2 emission from the Teide crater are available in the literature (Melián et al., 2012). In figure 8 we report the time series of diffuse CO_2 emission from the Teide crater from 1999 up to 2017. The marked increase in the CO_2 emission following the 2OSS is more than evident. It increased from an average background of 17.1 tons/day up to a maximum of 176.1 tons/day observed on February 2017. Hence, we can state that these geochemical observations strongly support a massive fluid injection as a causative mechanism of the 2OSS. The onset of the increase in the CO_2 emission, is delayed of at least one month with respect to the 2OSS. This can be simply explained taking into account the propagation of the magmatic fluids from a depth of about 8.6 km up to the surface, through advective-diffusive processes. A similar behavior has been observed in other volcanoes like Campi Flegrei in Italy (Chiodini et al., 2015) and Long Valley in USA (Shelly & Hill, 2011; Lewicki et al., 2014).

We can hypothesize different scenarios about the origin of this sudden, massive, fluid release. First of all, as pointed out by Fournier (1999), transient fluid release into the hydrothermal systems of volcanoes, may be related to the progressive accumulation of fluids on the top of a magma chamber followed by its rapid release, when the ductile layer at the roof of the magma chamber is no more able to retain them. A second scenario might imply the injection of basaltic magma within a crustal magma chamber, filled with a more differentiated magma, resulting from cooling at crustal depths. This would likely trigger convective mixing within the magma chamber (Longo et al., 2006) with subsequent release of exolved magmatic fluids. A third scenario could imply the intrusion of basaltic magma within the crust, with subsequent depressurization and liberation of magmatic fluids.

The presence of small sialic magma chambers beneath Teide volcano, has been postulated by different authors on the basis of petrological and vulcanological data (Martí and Gayer, 2009). Recent geophysical investigations using the magneto-telluric method, excluded the presence of large (>10 km^3) magma chambers at shallow depths (< 5 km) (Piña-Varas et al., 2018). The P-wave tomographic imaging of Tenerife as well, found no evidence of shallow magma chambers at least until depths of about 10 km (García-Yeguas et al., 2012). On the other hand, scattering imaging,

evidenced two possible reservoirs, one beneath the summit of Teide volcano at a depth of 1-4 km b.s.l. and another beneath the northern part of the island at a depth of 7-9 km b.s.l. (De Barros et al., 2012). While scattering imaging does not allow inferring about the current state of these anomalous bodies, which can consist of already solidified intrusions, a receiver function study suggests a low S-wave velocity zone starting at a depth of about 8 km (Lodge et al., 2012). Finally, an attenuation tomography study no found evidence of active magma chambers at shallow depth (Prudencio et al., 2015).

In our case we are considering a magma chamber located below the depth of the seismic source (8.6 km), so its presence would be compatible with current knowledge about the internal structure of Tenerife. Ground deformation in volcanoes is a strong indicator of the involvement of magma during a volcanic unrest (Dzurisin, 2006). Taking into account that before and after the 2OSS the GPS network of Tenerife did not record any deformation above the experimental error (about 1 cm) (see supplementary figure S5), we can constrain the maximum volumetric variation within the volcano. Fixing a source depth of 10 km, and using a simple Mogi point source model (Lisowski, 2007) we can establish an upper limit of the order of 10^{-3} km^3 to the volumetric variations of this virtual source. The total CO_2 emitted from the crater of Teide volcano alone, as diffuse degassing, reaches $3.2x10^7$ kg/day (excess with respect to a background of 17.1 tons/day). Considering the change in the solubility of CO_2 in a typical basaltic magma ascending from a depth of 25 km up to 10 km, this amount of CO_2 would imply a magma volume of the order of 10^{-2} km^3 (Shishkina et al., 2010). In this computation we have considered a fraction of 100% of CO_2 in the dissolved magmatic fluids and we have not considered the CO_2 emission from the fumaroles of Mt. Teide crater and diffuse degassing of the whole island. Hence the value of 10^{-2} km^3 should be strictly considered as a lower boundary, which is clearly incompatible with the absence of significant ground deformation. Furthermore, the seismicity pattern preceding and following the swarm does not show any relevant variation at depth below 10 km. On the other hand, we observed an increase of the seismicity in the shallower part of the volcano during 2017 (Fig. 9). This was probably triggered by the pressure increase in the hydrothermal system following the fluid injection. Seismicity induced by magmatic fluid injection within volcanic hydrothermal systems has been observed in other volcanoes like Mt. Vesuvius and Long Valley caldera as well (D'Auria et al., 2011; Shelly & Hill, 2011; D'Auria et al., 2013; Lewicki et al., 2014).

Conclusions

We analyzed seismic data related to the remarkable seismic swarm recorded on Tenerife on 2 October 2016. The results point to a source, located about 8.6 km depth, beneath the caldera of Las

Cañadas. The likely source mechanism is a transient discharge episode from a pressurized fluid reservoir into the hydrothermal system of the island. The marked increase in the diffuse CO_2 emission from the crater of Teide volcano, in the months following the swarm, provides additional evidence that the source has to be related with a massive magmatic fluid injection.

We considered three possible scenarios for explaining the source of this injection: release of fluid accumulated on the top of a magma chamber, convective mixing in a magma chamber triggered by the injection of mafic magma, or the ascent of a batch of basaltic magma. On the basis of ground deformation and seismicity data the third scenario seems unrealistic. However, we cannot yet discriminate between the first and the second with currently available data.

It is remarkable that both the first and the second scenarios imply the presence of a crustal magma chamber beneath Teide volcano at depths greater than 8.6 km. While this chamber has not yet been tomographically imaged, receiver function studies suggest at a zone of low S-wave velocity starting at a depth of about 8 km (Lodge et al., 2012). This suggests the possible presence of huge crustal magmatic reservoirs in Tenerife, at depths greater than 8-10 km.

These findings highlight the need for equipping the monitoring network of Tenerife with more sensitive instrumentation. In particular the continuous measurement of gravity changes would allow for better understanding of fluid types associated with any deformation and possibly detecting convective processes in a magma chamber (e.g., Carbone and Poland, 2012). Furthermore, the deployment of more sensitive geodetic instrumentation (strainmeters, high-resolution tiltmeters) would allow better constraining the volcanic processes involving volumetric variations at depth.

Acknowledgements

We acknowledge the associate editor G. Waite, the reviewer R. Matoza and another anonymous reviewer for their valuable suggestions which improved the quality of the manuscript.

This work has been possible thanks to the projects “Estudio de viabilidad técnica del uso combinado de métodos geofísicos (microsismicidad y magnetotelúrica) para la exploración geotérmica en la isla de Tenerife” (PTQ-15-08032), co-financed by the TORRES QUEVEDO Program of the R&D Spanish National Plan 2013-2016, VOLRISKMAC (MAC/3.5b/124; www.volriskmac.com), co-financed by the European Union MAC 2014-2020 Cooperation Transnational Programs, TFVOLCANO and TFASSISTANCE financed by Tenerife Innova 2016-2021 coordinated by the Tenerife 2030 Area of the Cabildo Insular de Tenerife.

The facilities of IRIS Data Services, and specifically the IRIS Data Management Center (https://ds.iris.edu/ds/nodes/dmc), were used for access to waveforms, related metadata, and/or derived products used in this study. IRIS Data Services are funded through the Seismological Facilities for the Advancement of Geoscience and EarthScope (SAGE) Proposal of the National Science Foundation under Cooperative Agreement EAR-1261681.

Seismic phases of CCAN and CBOL stations were downloaded by the web site of *Instituto Geográfico Nacional* (IGN): http://www.ign.es/web/ign/portal/vlc-catalogo

Onset times of individual events at station TNOR are available at: http://www.involcan.org/wp-content/uploads/2019/06/catalog_2oss.txt

We used the Python implementation of the RANSAC and DBSCAN algorithms, provided by the scikit-learn library (Pedregosa et al., 2011).

References

Almendros J, Ibáñez JM, Carmona E, Zandomeneghi D (2007) Array analyses of volcanic earthquakes and tremor recorded at Las Cañadas caldera (Tenerife Island, Spain) during the 2004 seismic activation of Teide volcano. J. Volc. Geoth. Res. 160:285–299

Ancochea, E., Fuster, J., Ibarrola, E., Cendrero, A., Coello, J., Hernan, F., ... & Jamond, C. (1990). Volcanic evolution of the island of Tenerife (Canary Islands) in the light of new K-Ar data. J. Volc. Geoth. Res., 44(3-4), 231-249.

Ancochea, E., Huertas, M. J., Cantagrel, J. M., Coello, J., Fúster, J. M., Arnaud, N., & Ibarrola, E. (1999). Evolution of the Cañadas edifice and its implications for the origin of the Cañadas Caldera (Tenerife, Canary Islands). J. Volc. Geoth. Res., 88(3), 177-199.

Anguita, F., & Hernán, F. (2000). The Canary Islands origin: a unifying model. J. Volc. Geoth. Res., 103(1-4), 1-26.

Bell, A. F., Hernandez, S., Gaunt, H. E., Mothes, P., Ruiz, M., Sierra, D., & Aguaiza, S. (2017). The rise and fall of periodic 'drumbeat'seismicity at Tungurahua volcano, Ecuador. Earth and Planetary Science Letters, 475, 58-70.

Bottiglieri, M., C. Godano, and L. D'Auria (2009), Distribution of volcanic earthquake recurrence intervals, J. Geophys. Res., 114, B10309, doi:10.1029/2008JB005942.

Carracedo, J. C., Badiola, E. R., Guillou, H., Paterne, M., Scaillet, S., Torrado, F. P., ... & Hansen, A. (2007). Eruptive and structural history of Teide Volcano and rift zones of Tenerife, Canary Islands. Geological Society of America Bulletin, 119(9-10), 1027-1051.

Carbone, D., & Poland, M. P. (2012). Gravity fluctuations induced by magma convection at Kīlauea Volcano, Hawai ‘i. Geology, 40(9), 803-806.

Chiodini, G., Vandemeulebrouck, J., Caliro, S., D'Auria, L., De Martino, P., Mangiacapra, A., & Petrillo, Z. (2015). Evidence of thermal-driven processes triggering the 2005–2014 unrest at Campi Flegrei caldera. Earth and Planetary Science Letters, 414, 58-67.

Chouet, B. (2003), Volcano seismology, Pure Appl. Geophys., 160, 739–788.

Chouet, B. A., & Matoza, R. S. (2013). A multi-decadal view of seismic methods for detecting precursors of magma movement and eruption. J. Volc. Geoth. Res., 252, 108-175.

Cusano, P., S. Petrosino, and G. Saccorotti (2008), Hydrothermal origin for sustained long-period (lp) activity at Campi Flegrei volcanic complex, Italy. J. Volc. Geoth. Res., 177, 1035–1044, doi:10.1016/j.jvolgeores.2008.07.019.

D'Auria, L., Giudicepietro, F., Aquino, I., Borriello, G., Del Gaudio, C., Lo Bascio, D., ... & Ricco, C. (2011). Repeated fluid-transfer episodes as a mechanism for the recent dynamics of Campi Flegrei caldera (1989–2010). J. Geoph. Res. Solid Earth, 116(B4).

D’Auria, L., Esposito, A. M., Bascio, D. L., Ricciolino, P., Giudicepietro, F., Martini, M., ... & Scarpato, G. (2013). The recent seismicity of Mt. Vesuvius: inference on seismogenic processes. Annals of Geophysics, 56(4), 0442.

De Barros, L., Martini, F., Bean, C. J., Garcia-Yeguas, A., & Ibáñez, J. (2012). Imaging magma storage below Teide volcano (Tenerife) using scattered seismic wavefields. Geophysical Journal International, 191(2), 695-706.

Domínguez I, del Fresno C., Rivera L. (2011) New insight on the increasing seismicity during Tenerife’s 2004 volcanic reactivation. J. Volc. Geoth. Res. 206:15–29

Dzurisin, D. (2006). Volcano deformation: new geodetic monitoring techniques. Springer Science & Business Media.

Ester, M., Kriegel, H. P., Sander, J., & Xu, X. (1996). A density-based algorithm for discovering clusters in large spatial databases with noise. In Kdd (Vol. 96, No. 34, pp. 226-231).

Fernández, J., Tizzani, P., Manzo, M., Borgia, A., González, P. J., Martí, J., ... & Prieto, J. F. (2009). Gravity-driven deformation of Tenerife measured by InSAR time series analysis. Geophysical Research Letters, 36(4).

Fischler, M. A., & Bolles, R. C. (1981). Random sample consensus: a paradigm for model fitting with applications to image analysis and automated cartography. Communications of the ACM, 24(6), 381-395.

Font, Y., Kao, H., Lallemand, S., Liu, C. S., & Chiao, L. Y. (2004). Hypocentre determination offshore of eastern Taiwan using the Maximum Intersection method. Geophysical Journal International, 158(2), 655-675.

Fournier, R. O. (1999), Hydrothermal processes related to movement of fluid from plastic into brittle rock in the magmatic-epithermal environment, Econ. Geol., 94(8), 1193–1211, doi:10.2113/gsecongeo.94.8.1193.

García-Yeguas, A., Koulakov, I., Ibáñez, J. M., & Rietbrock, A. (2012). High resolution 3D P wave velocity structure beneath Tenerife Island (Canary Islands, Spain) based on tomographic inversion of active-source data. Journal of Geophysical Research: Solid Earth, 117(B9).

Giudicepietro, F., Lo Bascio, D., Caputo, T., & D'Auria, L. (2010). Druk_Pkev: un programma per la costituzione di cataloghi supervisionati di eventi sismici ad elevata frequenza di accadimento. Rapporti Tecnici INGV (in Italian) http://istituto.ingv.it/images/collane-editoriali/rapporti%20tecnici/rapporti-tecnici-2010/rapporto124.pdf

Gottsmann J, Wooller L, Martí J, Fernández J, Camacho AG, González PJ, García A, Rymer H (2006) New evidence for the reawakening of Teide volcano. Geophys Res Let 33:L20311. doi:10.1029/2006GL027523

Kumagai, H., & Chouet, B. A. (1999). The complex frequencies of long-period seismic events as probes of fluid composition beneath volcanoes. Geophysical Journal International, 138(2), F7-F12.

Hernández, P. A., Pérez, N. M., Salazar, J. M., Nakai, S. I., Notsu, K., & Wakita, H. (1998). Diffuse emission of carbon dioxide, methane, and helium-3 from Teide Volcano, Tenerife, Canary Islands. Geophysical Research Letters, 25(17), 3311-3314.

Hernández P.A., Padilla G., Barrancos J., Melián G., Padrón E., Asensio-Ramos M., Rodríguez F., Pérez N., Alonso M. and Calvo D. (2017) Geochemical evidences of seismo-volcanic unrests at the NW rift

zone of Tenerife, Canary Islands, inferred from diffuse CO2 emission. Bull. Volcanol. (2017) 79: 30. https://doi.org/10.1007/s00445-017-1109-9

Hori, S., Fukao, Y., Kumazawa, M., Furumoto, M., & Yamamoto, A. (1989). A new method of spectral analysis and its application to the Earth's free oscillations: The “Sompi” method. Journal of Geophysical Research: Solid Earth, 94(B6), 7535-7553.

Hürlimann, M., Turon, E., & Marti, J. (1999). Large landslides triggered by caldera collapse events in Tenerife, Canary Islands. Physics and Chemistry of the Earth, Part A: Solid Earth and Geodesy, 24(10), 921-924.

Lewicki, J. L., Hilley, G. E., Shelly, D. R., King, J. C., McGeehin, J. P., Mangan, M., & Evans, W. C. (2014). Crustal migration of CO_2-rich magmatic fluids recorded by tree-ring radiocarbon and seismicity at Mammoth Mountain, CA, USA. Earth and Planetary Science Letters, 390, 52-58.

Lisowski, M. (2007). Analytical volcano deformation source models. In Volcano deformation (pp. 279-304). Springer, Berlin, Heidelberg.

Lodge, A., Nippress, S. E. J., Rietbrock, A., García-Yeguas, A., & Ibáñez, J. M. (2012). Evidence for magmatic underplating and partial melt beneath the Canary Islands derived using teleseismic receiver functions. Physics of the Earth and Planetary Interiors, 212, 44-54.

Lomax, A., Virieux, J., Volant, P., & Berge-Thierry, C. (2000). Probabilistic earthquake location in 3D and layered models. In Advances in seismic event location (pp. 101-134). Springer, Dordrecht.

Longo, A., Vassalli, M., Papale, P., & Barsanti, M. (2006). Numerical simulation of convection and mixing in magma chambers replenished with CO_2-rich magma. Geophysical research letters, 33(21).

Martí, J., & Geyer, A. (2009). Central vs flank eruptions at Teide–Pico Viejo twin stratovolcanoes (Tenerife, Canary Islands). Journal of Volcanology and Geothermal Research, 181(1-2), 47-60.

Martí J, Ortiz R, Gottsmann J, Garcia A, De La Cruz-Reina S (2009) Characterising unrest during the reawakening of the central volcanic complex on Tenerife, Canary Islands, 2004–2005, and implications Tenerife (Canary Islands) in the light of new K-Ar data. J Volcanol Geotherm Res 44:231–249

Martini, M., Giudicepietro, F., D’Auria, L., Esposito, A. M., Caputo, T., Curciotti, R., ... & Peluso, R. (2007). Seismological monitoring of the February 2007 effusive eruption of the Stromboli volcano. Annals of Geophysics.

Matoza, R. S., Garcés, M. A., Chouet, B. A., D'Auria, L., Hedlin, M. A., Groot-Hedlin, D., & Waite, G. P. (2009). The source of infrasound associated with long-period events at Mount St. Helens. Journal of Geophysical Research: Solid Earth, 114(B4).

Matoza R.S., and B.A. Chouet (2010). Subevents of long-period seismicity: Implications for hydrothermal dynamics during the 2004-2008 eruption of Mount St. Helens, J. Geophys. Res., 115, B12206, doi:10.1029/2010JB007839

Melián, G., Tassi, F., Pérez, N., Hernández, P., Sortino, F., Vaselli, O., ... & Rodríguez, F. (2012). A magmatic source for fumaroles and diffuse degassing from the summit crater of Teide Volcano (Tenerife, Canary Islands): a geochemical evidence for the 2004–2005 seismic–volcanic crisis. Bulletin of Volcanology, 74(6), 1465-1483.

Morrissey, M. M., & Chouet, B. A. (1997). A numerical investigation of choked flow dynamics and its application to the triggering mechanism of long-period events at Redoubt Volcano, Alaska. Journal of Geophysical Research: Solid Earth, 102(B4), 7965-7983.

Nakano, M., Kumagai, H., Kumazawa, M., Yamaoka, K., & Chouet, B. A. (1998). The excitation and characteristic frequency of the long-period volcanic event: An approach based on an inhomogeneous autoregressive model of a linear dynamic system. Journal of Geophysical Research: Solid Earth, 103(B5), 10031-10046.

Pérez, N. M., Hernández, P. A., Padrón, E., Melián, G., Marrero, R., Padilla, G., ... & Nolasco, D. (2007). Precursory subsurface ^{222}Rn and ^{220}Rn degassing signatures of the 2004 seismic crisis at Tenerife, Canary Islands. Pure and Applied Geophysics, 164(12), 2431-2448.

Pedregosa, F., Varoquaux, G., Gramfort, A., Michel, V., Thirion, B., Grisel, O., ... & Vanderplas, J. (2011). Scikit-learn: Machine learning in Python. Journal of machine learning research, 12(Oct), 2825-2830.

Pérez, N. M., Hernández, P. A., Padrón, E., Melián, G., Nolasco, D., Barrancos, J., ... & Chiodini, G. (2013). An increasing trend of diffuse CO_2 emission from Teide volcano (Tenerife, Canary Islands): geochemical evidence of magma degassing episodes. Journal of the Geological Society, 170(4), 585-592.

Piña-Varas, P., Ledo, J., Queralt, P., Marcuello, A., & Perez, N. (2018). On the detectability of Teide volcano magma chambers (Tenerife, Canary Islands) with magnetotelluric data. Earth, Planets and Space, 70(1), 14.

Prudencio, J., Ibáñez, J. M., Del Pezzo, E., Martí, J., García-Yeguas, A., & De Siena, L. (2015). 3D attenuation tomography of the volcanic island of Tenerife (Canary Islands). Surveys in Geophysics, 36(5), 693-716.

Romero C. (1991) Las manifestaciones volcánicas históricas del archipiélago canario (2 vols). Gobierno de Canarias, Sta. Cruz de Tenerife, Spain (in Spanish)

Shelly, D. R., & Hill, D. P. (2011). Migrating swarms of brittle-failure earthquakes in the lower crust beneath Mammoth Mountain, California. Geophysical Research Letters, 38(20).

Shishkina, T. A., Botcharnikov, R. E., Holtz, F., Almeev, R. R., & Portnyagin, M. V. (2010). Solubility of H_2O-and CO_2-bearing fluids in tholeiitic basalts at pressures up to 500 MPa. Chemical Geology, 277(1-2), 115-125.

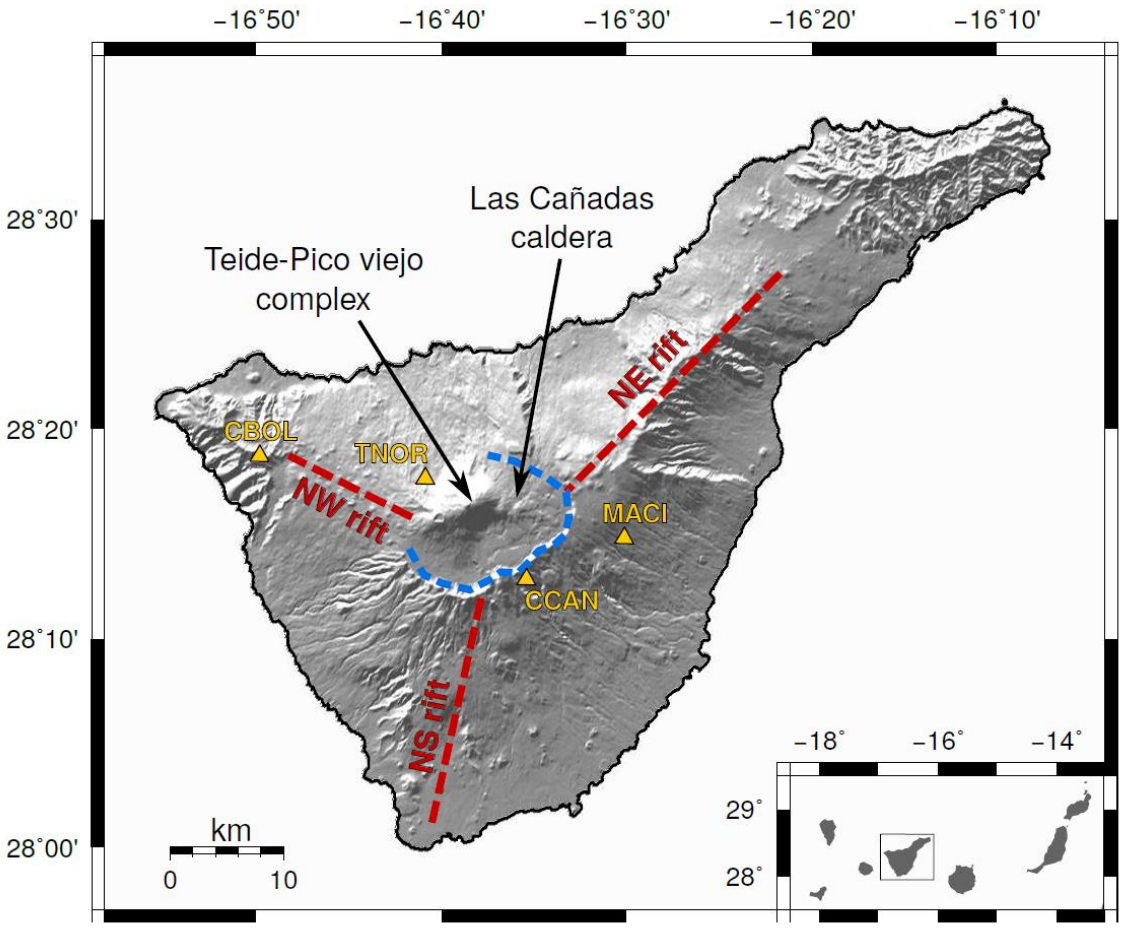

Figure 1 – Basic volcano-tectonic features of Tenerife. Red dashed lines: volcanic rifts of Tenerife. Blue dashed line: approximate limits of Las Cañadas caldera. Yellow triangles: seismic stations used in this work.

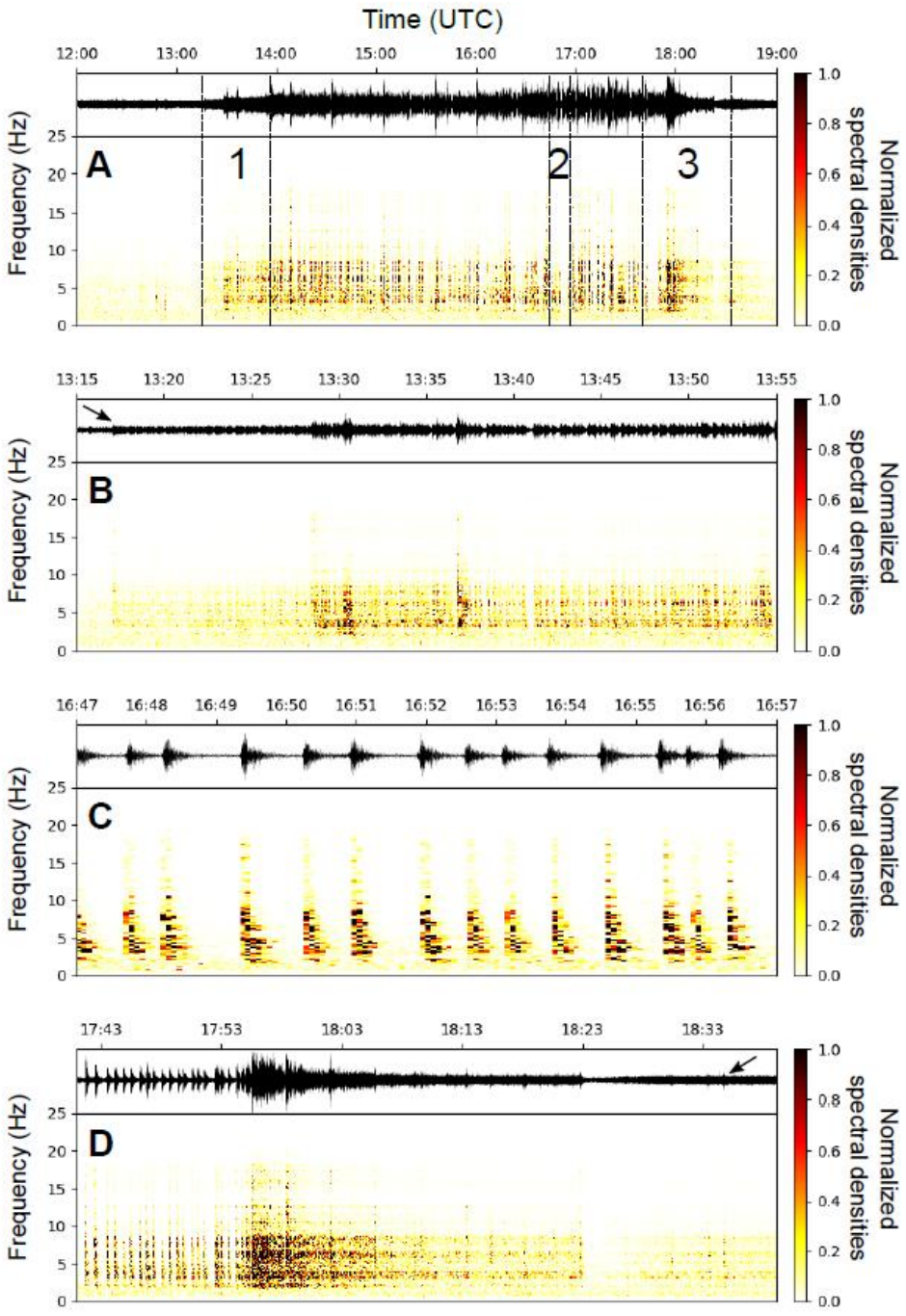

Figure 2 – Seismograms and spectrograms of the 2OSS from the N-S component of the seismic station TNOR. A) Normalized seismogram and corresponding spectrogram for the whole seismic swarm, from 12:00 to 19:00 UTC of 2 October 2016. B) Same as (A) for the onset of the swarm (interval 13:15 to 13:55 UTC, marked as 1 in panel A). The small arrow indicates the onset of the swarm at 13:16 UTC. C) Same as (A) for the central part of the swarm (interval 16:47 to 16:57 UTC, marked as 2 in panel A). D) Same as (A) for the final part of the swarm (interval 17:40 to 18:38 UTC, marked as 3 in panel A). The small arrow indicates last discrete event at 18:34 UTC.

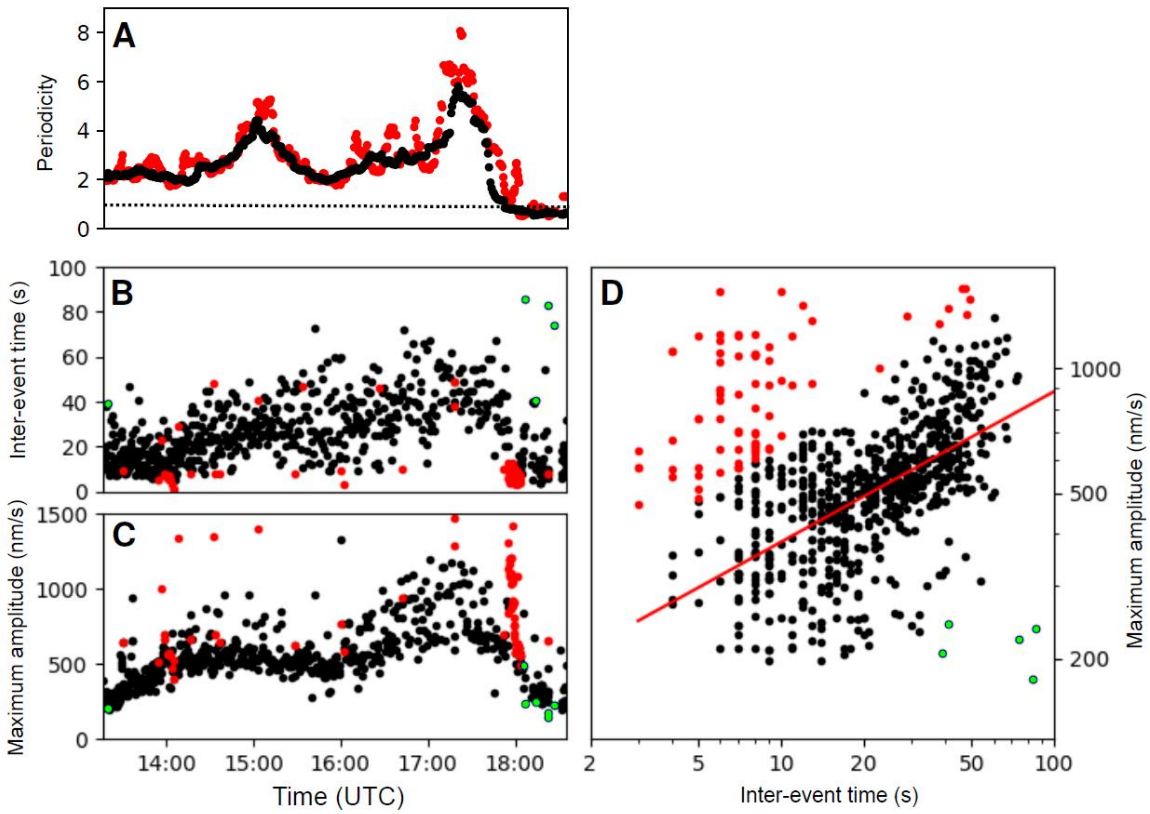

Figure 3 – Statistical relationship between inter-event times and amplitudes of discrete events. A) Periodicity computed over windows of 10 minutes (red points) and 30 minutes (black points). The dotted line marks the value of 1. B) Inter-event times between discrete events. C) Maximum amplitudes of discrete events. D) Linear fit between the logarithm of the amplitude and the logarithm of the inter-event time. The red line represents the best-fit solution found by the RANSAC algorithm. Red and green points in panels B, C and D are outliers detected by the RANSAC algorithm and excluded from the fit.

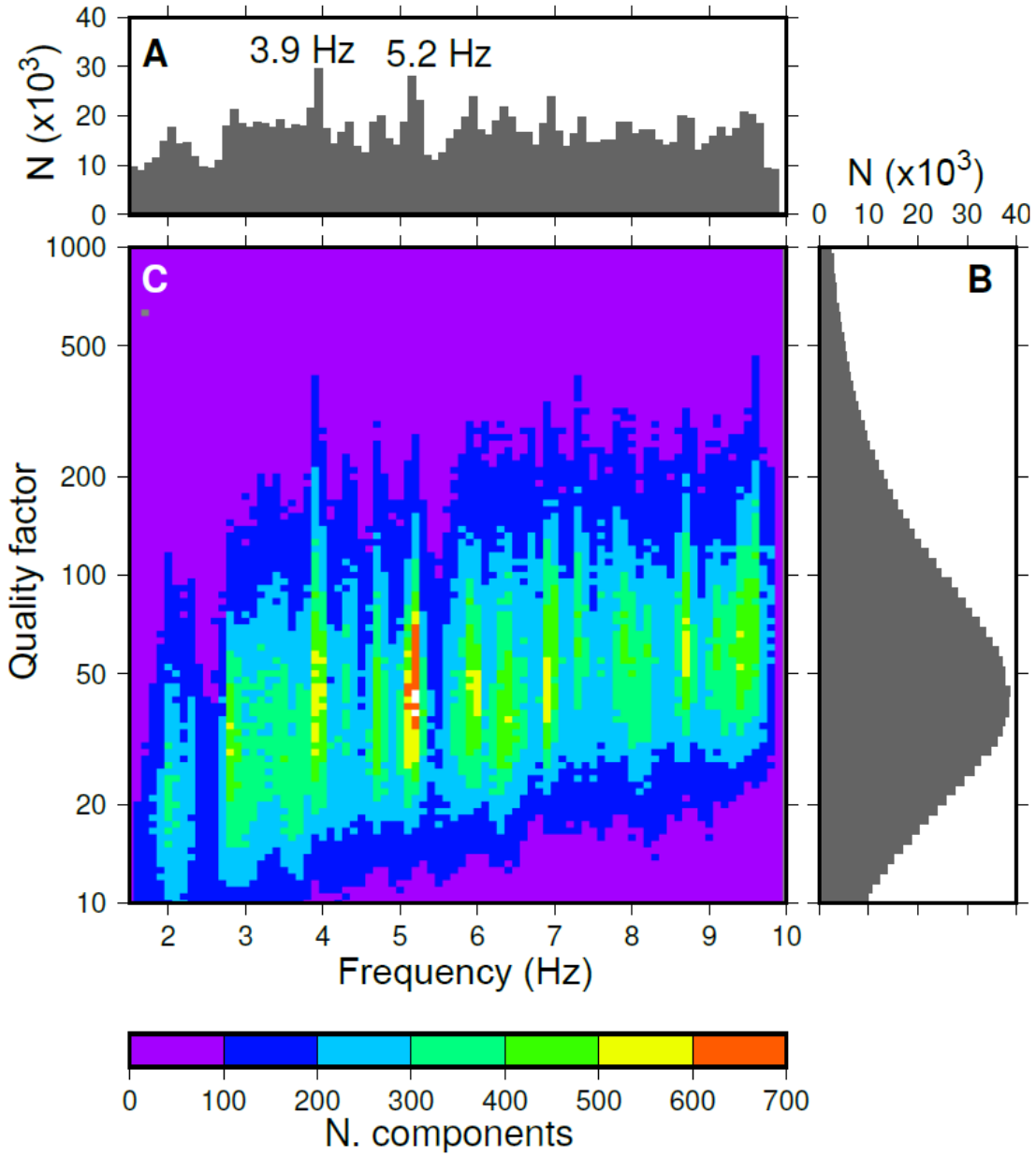

Figure 4 – Complex spectral analysis. A) Histogram of the frequencies of the spectral components detected by the Sompi method for all the discrete events. The bin width is of 0.1 Hz. We reported the value of the two most prominent peaks on the histogram. B) Same as for (A) for the quality factors. The bin width is of 0.03 for the logarithm of Q. C) Density map for the complex spectral components. The bin width is the same as for the histograms.

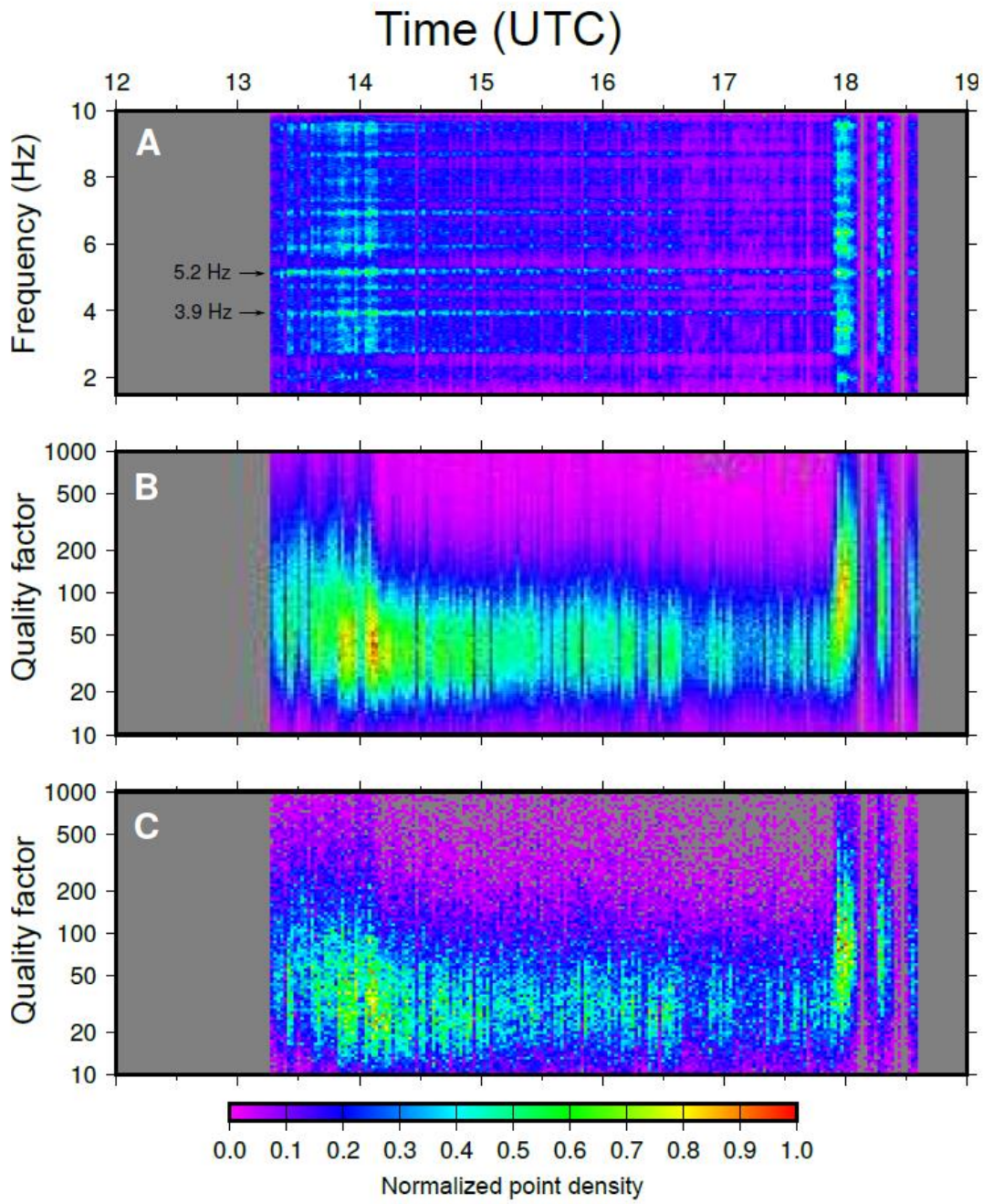

Figure 5 – Temporal evolution of the complex frequencies. A) Temporal evolution of the frequencies. We reported the two most relevant peaks in the histogram of figure 4A. B) Temporal evolution of the quality factors. C) Temporal evolution of the quality factors only for the components having a frequency of 3.9$\pm$0.1 Hz.

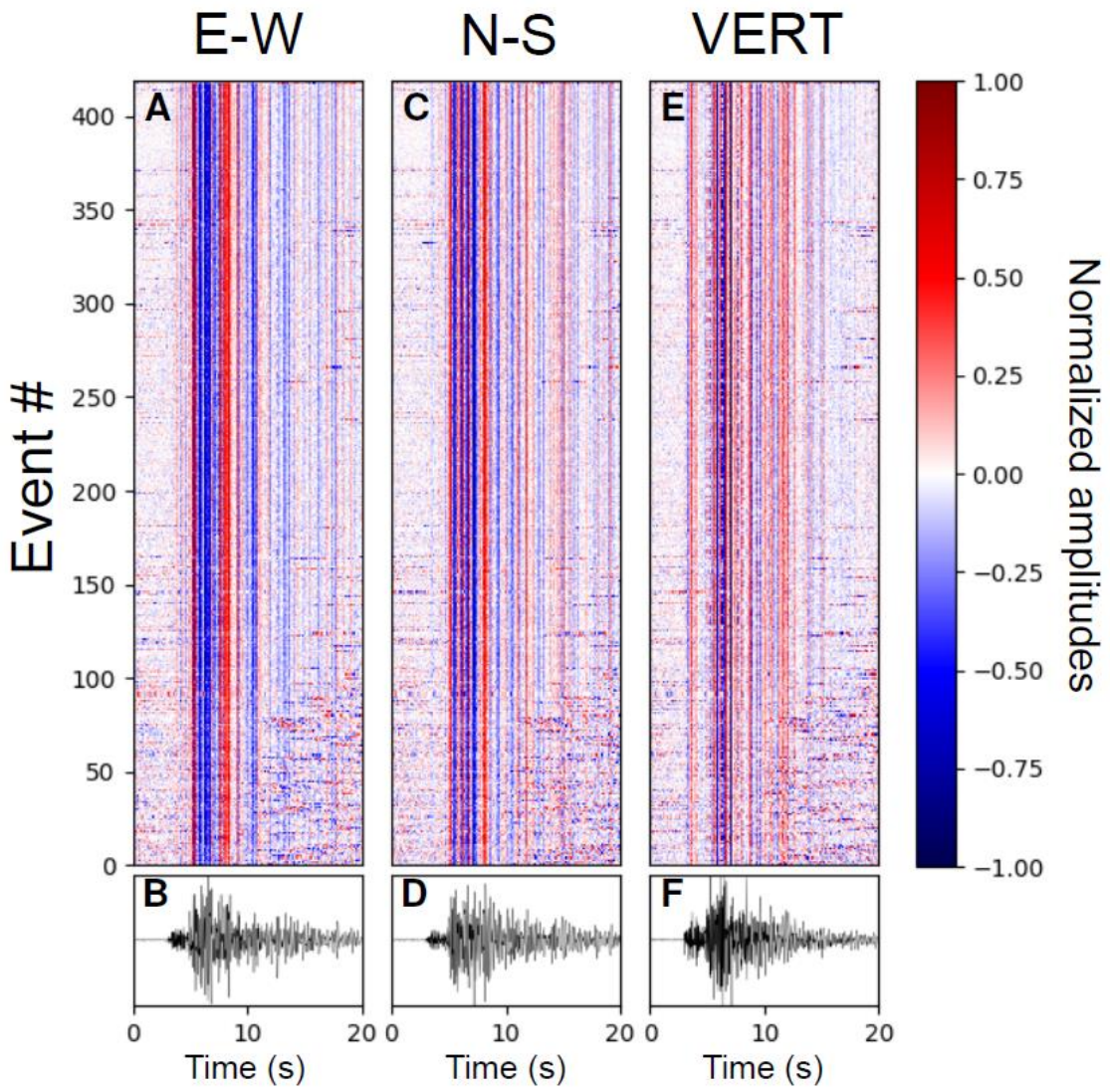

Figure 6 – Stacking of event waveforms. A) Representation of the normalized waveforms for the EW component of TNOR. B) Stack of the waveforms shown in panel A. C) and D) same as (A) and (B) for the NS component. E) and F) same as (A) and (B) for the vertical component. The Event # is ordered on the basis of the onset time.

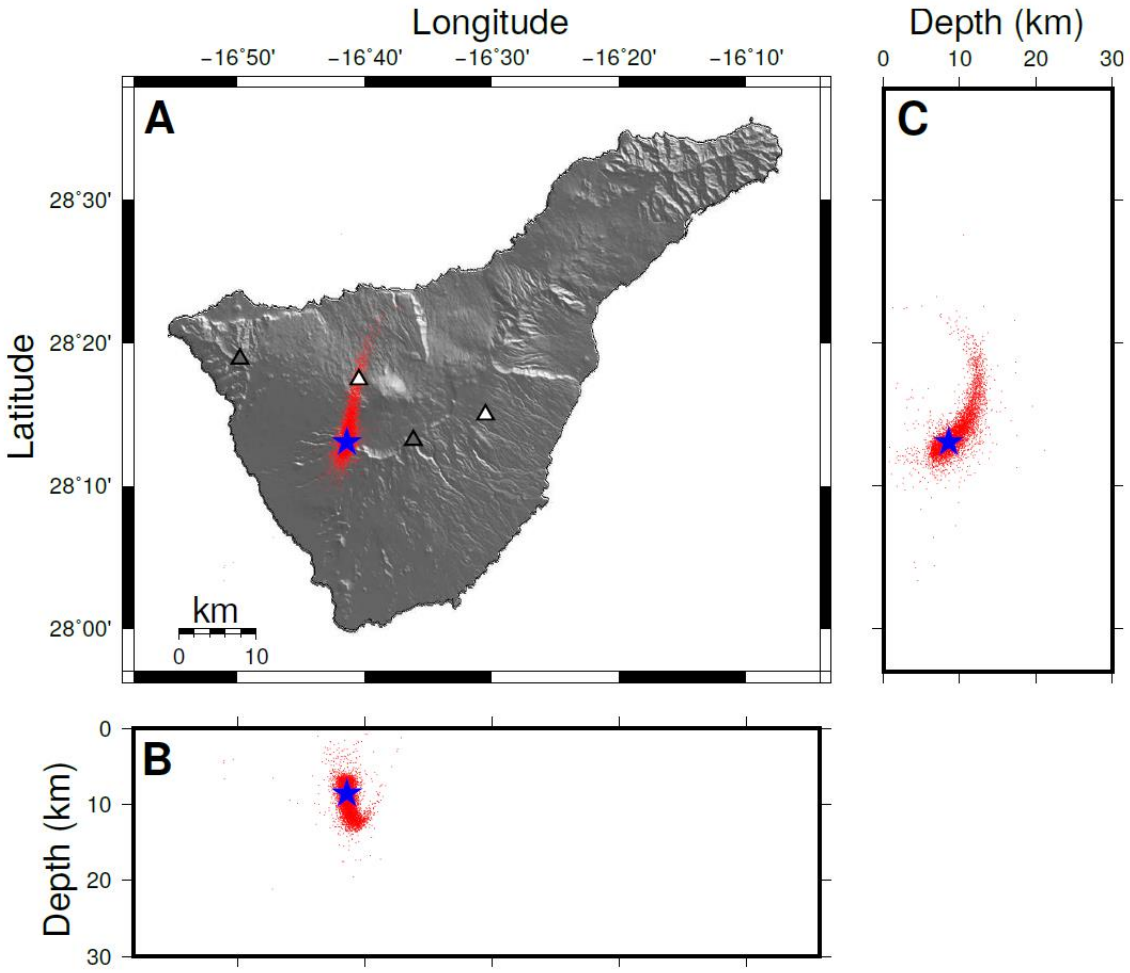

Figure 7 – Hypocenter location. A) The map shows the location of the stations used for the hypocenter determination. White triangles indicate stations for which full waveforms have been used, while gray triangles refer to station for which only picked phases were available. The red points density is proportional to the "a posteriori" probability density function. The blue star shows the location of the maximum likelihood hypocenter. B) and C) represent respectively the projection of the p.d.f. and of the hypocenter location along EW and NS cross-sections respectively.

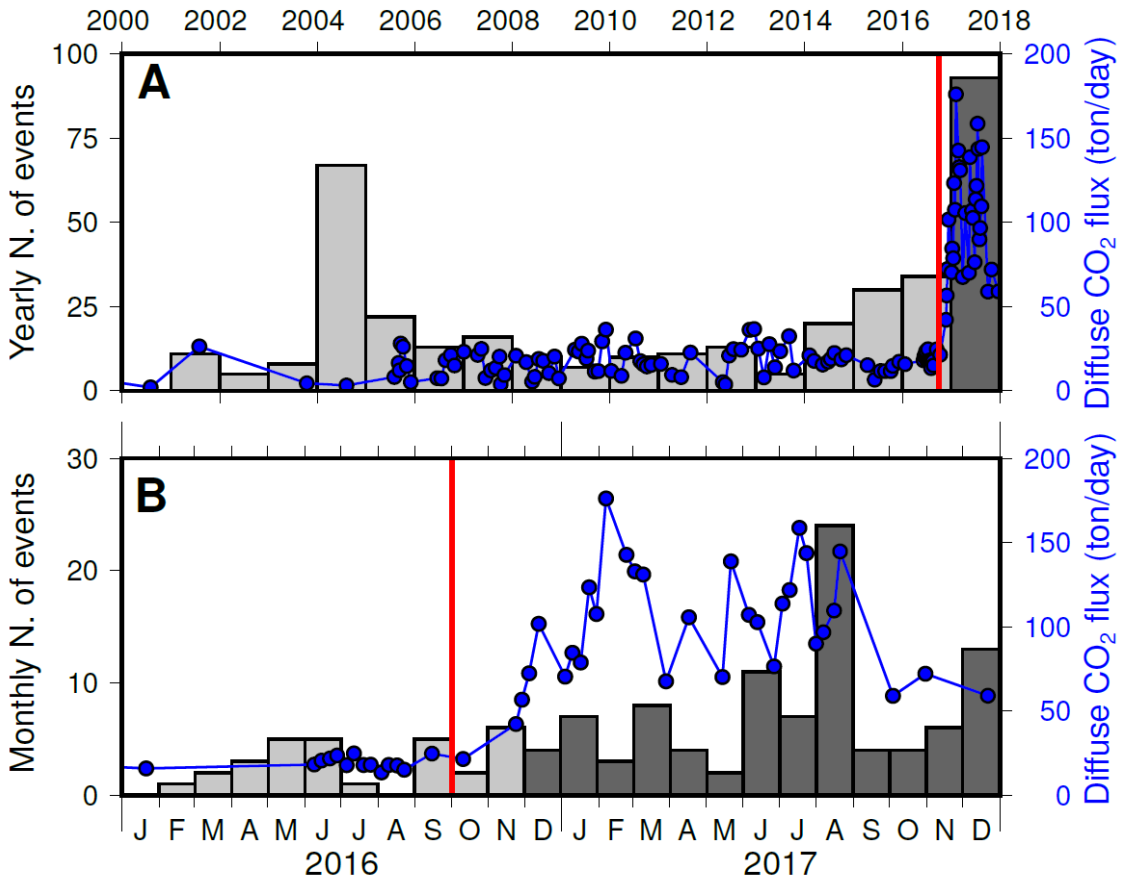

Figure 8 – Temporal evolution of the diffuse CO_2 emission from the crater of Teide volcano and the volcano-tectonic seismicity rates. A) Blue points: the temporal evolution of the CO_2 emission since the year 2000; histogram: yearly number of volcano-tectonic (VT) earthquakes on the island of Tenerife and its surrounding. The red line marks the occurrence of the 2OSS. B) Same as (A) for the interval 2016-2017. The histogram represents the monthly number of VT earthquakes. The source of the data in gray is from the on-line catalogue of IGN, while those in black have been detected and located by the *Red Sísmica Canaria* managed by INVOLCAN.

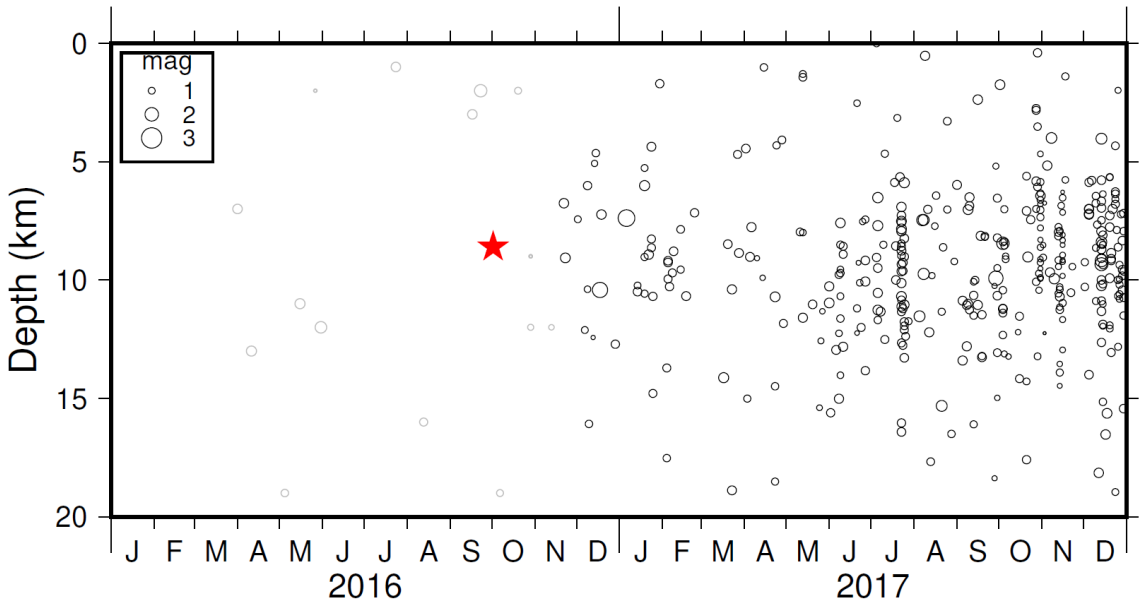

Figure 9 – Temporal evolution of the hypocenter depths of volcano-tectonic earthquakes located within a radius of 15 km from the 2OSS epicenter. The size of the circles is proportional to the magnitude as indicated in the inset on the upper left of the figure. The red star marks the 2OSS. The source of the events in gray is from the on-line catalogue of IGN, while the events in black have been detected and located by the *Red Sísmica Canaria* managed by INVOLCAN.